Collision, Coalescence and Breakup of Raindrops. Part II: Parameterization of Fragment Size Distributions

T. B. LOW[1] AND ROLAND LIST[2]

Department of Physics, University of Toronto, Toronto, Ontario M5S 1A7, Canada

(Manuscript received 16 November 1981, in final form 1 March 1982)

ABSTRACT

The experimental drop collision/breakup results of Low (1977) and Low and List (1982) and McTaggart-Cowan and List (1975b), taken at laboratory pressure and terminal drop speeds, were parameterized for future use in cloud and precipitation modeling. The primary analyses of the 10 representative raindrop pairs were based on the three main geometric shapes generally assumed by the drop pairs after their initial contact and before breakup (or coalescence): filaments, sheets and disks. Relationships for the average total fragment number for each category are given. The fragment number distributions resulting from the collisions in each classification were fitted as sums of normal and log-normal distributions with the parameters of each distribution being related to the drop sizes and physical quantities derived from them (like the collision kinetic energy, CKE).

Each collision was then weighted according to the individual contribution and summed to give the probability of occurrence of each breakup type. The weighting functions were based on the CKE of each pair as determined in the center of drop mass frame. With the newly established coalescence efficiencies for raindrop pairs by Low and List (1982) the collision breakup equations were expanded into general overall equations for all drop pairs as expected in natural rain.

1. Introduction

As raindrops fall and interact in the atmosphere, the collision between individual drop pairs may result in coalescence, breakup or bouncing. At their terminal velocities in free air, raindrops (diameter $> 200\ \mu m$) possess sufficient momentum to overcome any intervening air film which would produce bouncing [McTaggart-Cowan and List, 1975 (hereafter referred to as M-L); and Low, 1977 and Low and List, 1982 (referred to as LL for both references)]. Coalescence produces a single drop of a size corresponding to the mass sum of the colliding drops. Breakup alters the raindrop size spectrum by producing a distribution of varying sizes for the resulting fragments.

While the previous studies (see literature review by LL) concentrated on the relative velocities of motion—even off the vertical—it was found by M-L that at terminal velocity, the breakup mechanisms took place more frequently than at lower speeds because the aerodynamic flow at terminal velocity represents an important contribution to the force balance during collision. The experiments of M-L represented a major advance in that their collision experiments were performed with the drops falling nearly vertical at their terminal velocities. These results were confirmed by LL which not only verified the collision data of M-L but also extended the sizes of drops studied to cover essentially the entire range of the raindrop size spectrum.

The combined results of M-L and LL produced a total of 1473 individual collisions between 10 drop pairs. The sizes of drops used ranged from 0.46 to 0.0395 cm in diameter. The large number of collisions achieved and fragment sizes measured for breakup permitted a description of the collision results in terms of average fragment number distributions for the resultant drop sizes. This paper parameterizes these frequency distributions for modeling purposes.

2. Fragment number densities

In order to implement the collision data into any numerical models, it is necessary to express in explicit terms the average outcome of a collision between any drop pair, i.e., the number frequency of a particular fragment size being produced in an average collision must be known. The equations fitted to the first breakup data set of M-L by List and Gillespie (1976) did this by treating the collisions in an averaged way, a task which was simplified by the assumption of no coalescence for drops of size >0.1 cm in diameter and the absence of any fragment drops with sizes <0.05 cm. However, the data of LL with smaller sizes revealed that this treatment is too simplistic.

[1] Present affiliation: The Environmental Applications Group Limited, 114 Avenue Road, Toronto, Ontario M5R 2H4, Canada.
[2] Present affiliation: WMO, Geneva, Switzerland.

0022-4928/82/071607-12$07.00

It was further assumed that the breakup phenomenon can be better understood if the analyses are applied to the individual breakup groups first. The total view of the collision process can then be gained by summing over the individual contributions. The subscripts f, s, d and b will be used henceforth to indicate values attributed to the filament, sheet, disk and the sum of the breakup modes, respectively, while the lack of a subscript will denote the overall result of a collision, including coalescence. Any collision resulting in two or more fragments is considered to be breakup, regardless of the fragment sizes. The formalism applied was developed for the data taken experimentally.

The representation $P_i(D_i)$ will be used to give the average number of fragments of diameter D_i in the interval $D_i \pm \Delta D_i/2$ for one collision between two drops of size D_L (large drop) and D_S (small drop) as averaged over many (at least 100) collisions, i.e.,

$$P_i(D_i) = \frac{\text{Total number of fragments of size } D_i (=N_i)}{\text{Total number of collisions}} \times \frac{1}{\Delta D_i}. \quad (2.1)$$

Thus for a continuous description of the fragment number, $P_i(D_i)$ is the number density function while the integral

$$P(D_i) = \int_{-\infty}^{D_i} P_i(D)dD \quad (2.2)$$

expresses the fragment number distribution. If $P_{fi}(D_i)$, $P_{si}(D_i)$, $P_{di}(D_i)$ represent the fragment number densities for filaments, sheets and disks, respectively, then the density function for each breakup mode can be defined similarly to Eq. (2.1), but it is prorated now to the total number of collisions leading to breakup. Thus, if C_b represents the total number of collisions followed by breakup, then the total numbers of collisions of each type are C_f, C_s, C_d, with the total

$$C_b = C_f + C_s + C_d. \quad (2.3)$$

If $N_{fi\Delta}$ is the number of fragments of size D_i per size interval ΔD_i for filament breakups, then $N_{si\Delta}$ and $N_{di\Delta}$ can be used for sheets and disks and the sum of the breakups [Eq. (2.1)] can now be subdivided into

$$\left.\begin{aligned} P_{fi} &= N_{fi\Delta}C_f^{-1} \\ P_{si} &= N_{si\Delta}C_s^{-1} \\ P_{di} &= N_{di\Delta}C_d^{-1} \end{aligned}\right\}. \quad (2.4)$$

In order to determine the contribution of each density function to the overall breakup fragment number distribution, the fraction R_j (j represents the type of breakup, i.e., $j = f, s, d$) of the total breakup that each type represents must be known. Thus,

$$R_f = \frac{\text{Number of filament breakups}}{\text{Total number of breakup collisions}} = \frac{C_f}{C_b}. \quad (2.5)$$

Similarly $R_s = C_sC_b^{-1}$ and $R_d = C_dC_b^{-1}$.

The overall breakup number distribution function can then be expressed as the sum of its parts, i.e.,

$$P_{bi} = R_fP_{fi} + R_sP_{si} + R_dP_{di}. \quad (2.6)$$

This can be verified by substituting Eqs. (2.4) and (2.5) into (2.6).

3. Average fragment number for each breakup type

a. Basic equations

Equations are required to describe the total number of fragments of all sizes for all types of collisions. Since $P_i(D_i)$ is the fragment number density for size D_i per size interval per collision, the area under the histogram for the discrete measurements would be the summation of Eq. (2.1) over all sizes, i.e.,

$$\sum_i P_i(D_i)\Delta D_i = C^{-1} \sum_i N_i = \bar{F}. \quad (3.1)$$

The right side of Eq. (3.1) represents the average total number of fragments $\bar{F}$ produced in a collision. Adding, for breakup, the suffix j in the appropriate places gives the terms for $\bar{F}_j$, so that for all breakup collisions we have

$$\bar{F}_b = \sum_j R_j\bar{F}_j = R_f\bar{F}_f + R_s\bar{F}_s + R_d\bar{F}_d. \quad (3.2)$$

To parameterize the fragment number distribution or density functions for the breakup and coalescence collisions, the average number of fragments must be expressed in functional form and the $\bar{F}_j$ must be preserved in all fittings of the fragment distributions as measured by LL. This is also the case for Eq. (3.2).

b. Filament breakup

For the filament breakup, an empirical equation was developed which fits the measured values of $\bar{F}_f$ of LL. For each small drop D_S, the value of $\bar{F}_f$ was divided into two parts. The first varied according to a power law of the form

$$\bar{F}_{f1} = [-2.25 \times 10^4(D_L - 0.403)^2 - 37.9]D_S^{2.5} + 9.67(D_L - 0.170)^2 + 4.95, \quad (3.3)$$

where $[D_S]$ is in centimeters.

This equation is valid for $D_S \geq D_{S0}$, with the further restriction that $\bar{F}_f \geq 2$, since each breakup must produce at least two fragments. In this and all following equations values for diameters D_L and D_S are to be expressed in centimeters.

D_{S0} is the limiting value of D_S below which the

TABLE 1. Average fragment numbers for the different breakups, as measured experimentally and calculated through the parameterization schemes developed in Sections 2 and 3; drop pairs are listed in increasing order of magnitude of the collision kinetic energy. $\bar{F}_f$ stands for filament, $\bar{F}_s$ for sheet and $\bar{F}_d$ for disk breakup; σ is the standard deviation.

Drop pair		Experimental			Calculated		
No.	Diameters (cm)	$\bar{F}_f \pm \sigma$	$\bar{F}_s \pm \sigma$	$\bar{F}_d \pm \sigma$	$\bar{F}_f$	$\bar{F}_s$	$\bar{F}_d$
1	0.18; 0.0395	2.98 ± 0.41			3.08		
2	0.40; 0.0395	3.35 ± 0.38			3.08		
3	0.44; 0.0395	2.89 ± 0.38			3.08		
4	0.18; 0.0715	4.55 ± 0.52	2.27 ± 0.65		4.55	2.01	
5	0.18; 0.10	2.48 ± 0.28	2.23 ± 0.60		2.48	2.17	
6	0.30; 0.10	5.25 ± 0.65	5.72 ± 1.97	3.68 ± 1.49	6.21	5.26	3.41
7	0.36; 0.10	7.41 ± 1.29	8.81 ± 2.35	7.82 ± 3.26	7.41	7.94	9.72
8	0.46; 0.10	8.44 ± 1.49	10.58 ± 3.76	14.58 ± 10.30	8.44	10.74	14.24
9	0.36; 0.18	6.57 ± 1.37	9.94 ± 3.45	23.53 ± 7.39	6.57	9.15	20.81
10	0.46; 0.18	7.27 ± 1.27	10.73 ± 3.60	28.27 ± 17.36	7.27	10.90	29.70

energy differences in the collisions with drops of size D_L produce fragment numbers which are dependent only on the size of D_S, i.e., the size ratio D_L/D_S has become so large in the CKE calculations that the actual size of D_L is unimportant. This infers that the terminal velocity of D_L can be essentially regarded as a constant of large magnitude.

For $D_S < D_{S0}$, the relationship of $\bar{F}_f$ to D_S is simply

$$\bar{F}_{f2} = a'' D_S^{b''} + 2, \tag{3.4}$$

with $a'' = 1.02 \times 10^4$ and $b'' = 2.83$.

The limiting value of D_S is calculated from the intersection of $\bar{F}_{f1}$ and $\bar{F}_{f2}$, i.e.,

$$D_{S0} = (\bar{F}_{f1}/b'')^{1/a''}. \tag{3.5}$$

Eqs. (3.3)–(3.5) maintain the result that both at the top end of the drop sizes where D_S approaches D_L and at the lower end where D_S becomes small, $\bar{F}_f$ has a limiting value of 2. In both cases the collisions become less energetic and, in all likelihood, result in a filament breakup with original drops as fragments. The experimental and calculated values are shown in Table 1.

c. *Sheet breakup*

To determine the average fragment number for each sheet breakup, the area under P_{si} must be calculated from experiments and empirical equations describing the distributions. This area is equal to $\bar{F}_s$, the average number of fragments produced from a sheet breakup. $\bar{F}_s$ was found to be a function of the total surface energy S_T according to

$$S_T = \pi\sigma(D_L^2 + D_S^2), \tag{3.6}$$

where $\sigma = 7.28 \times 10^{-2}$ N m^{-1} is the surface tension.

If the colliding drops are large, the greater surfaces can supply more energy toward the formation of new drop fragments as the colliding drops become disrupted. From the experimental breakup data, $\bar{F}_s$ reaches a limiting value as the drop sizes either increased or decreased. The lower limit was 2, so that

$$\bar{F}_s = 5 \operatorname{erf}\left(\frac{S_T - 2.53 \times 10^{-6}}{1.85 \times 10^{-6}}\right) + 6, \tag{3.7}$$

with $[S_T]$ in joules. Thereby, use was made of the error function

$$\operatorname{erf}(y_0) = \frac{2}{\sqrt{\pi}} \int_0^{y_0} e^{-y^2} dy. \tag{3.8}$$

The experimental and calculated values of $\bar{F}_s$ are listed in Table 1.

d. *Disk breakups*

The fragments resulting from disk collisions $\bar{F}_d$ were the most numerous and most variable in both size and number. It was found that $\bar{F}_d$ was closely related to the CKE [J] by

$$\bar{F}_d = 297.5 + 23.7 \ln\text{CKE}, \tag{3.9}$$

with the restriction that $\bar{F}_d \geq 2$. It was assumed that as CKE decreased, the fragment numbers would also decrease until the disk collisions—if they still occurred—would produce only two fragments in case of breakup; otherwise coalescence would occur. From Eq. (3.9) $\bar{F}_d$ must equal 2 for all CKE < 3.65 μJ. The measured and fitted values are also shown in Table 1.

4. Distribution functions for fragment numbers

a. *Filament breakup*

The fragment distribution function in each collision mode must be determined to give the number of any size of fragment occurring in either a filament, sheet, or disk breakup.

In all filament breakups, the original two drops usually reappeared in some fashion as recognizable remnants of the colliding drops. It was decided to represent the fragment number density function for

those two entities as two separate Gaussian functions with the area under the curve being unity for both fragments. The values for the large drop fragment, measured or calculated from mass conservation (LL), both indicated that the peak of the distribution would be centered at D_L. A cutoff in the number density function was imposed at the coalesced drop size, i.e.,

$$D_{\text{coal}} = (D_L^3 + D_S^3)^{1/3}. \tag{4.1}$$

For the density function $P_{f1}(D_i)$ around D_L the area under the curve is given by

$$\int_{-\infty}^{D_{\text{coal}}} P_{f1}(D_i)dD_i = 1, \tag{4.2}$$

while P_{f1} can be expressed as

$$P_{f1}(D_i) = H_{f1} \exp\left[-\frac{1}{2}\left(\frac{D_i - \mu}{\sigma_{f1}}\right)^2\right], \tag{4.3}$$

where σ_{f1} is the standard deviation of P_{f1}, and H_{f1} is a constant chosen to represent the peak value of P_{f1}; μ is the mode of the distribution and is equal to D_L. By specifying these parameters, the distribution is explicitly defined in terms of the dependent variable σ_{f1}. From the experiments the peak was found to be

$$H_{f1} = 50.8D_L^{-0.718}. \tag{4.4}$$

Eqs. (4.2), (4.3) and (4.4) can now be rewritten as

$$\int_{-\infty}^{X_0} \sqrt{2}\sigma_{f1}e^{-X^2}dX = H_{f1}^{-1}, \tag{4.5}$$

with

$$X_0 = (D_{\text{coal}} - D_L)(\sqrt{2}\sigma_{f1})^{-1}, \tag{4.6}$$

$$X = (D_i - D_L)(\sqrt{2}\sigma_{f1})^{-1}. \tag{4.7}$$

In terms of the error function [Eq. (3.8)] Eq. (4.5) becomes

$$H_{f1}^{-1} = 0.5\,\pi\left[1 + \text{erf}\left(\frac{D_{\text{coal}} - D_L}{\sqrt{2}\sigma_{f1}}\right)\right]. \tag{4.8}$$

This gives an expression for σ_{f1} which can be solved by linear iteration with an initial guess of

$$\sigma_{f1,1} = H_{f1}^{-1} \tag{4.9}$$

and successive approximations of

$$\sigma_{f1,i+1} = \frac{1}{H_{f1}}\sqrt{\frac{2}{\pi}}\left[1 + \text{erf}\left(\frac{D_{\text{coal}} - D_L}{\sqrt{2}\sigma_{f1,i}}\right)\right]^{-1}. \tag{4.10}$$

The Gaussian curve around the small drop fragment was evaluated in the same manner with

$$\int_{-\infty}^{\infty} P_{f2}(D_i)dD_i = 1, \tag{4.11}$$

where $P_{f2}(D_i)$ is the density function centered around D_S. $P_{f2}(D_i)$ is in the same form as Eq. (4.3). The peak and standard deviation are H_{f2} and σ_{f2}, respectively. The mode is now D_S and the peak is given by

$$H_{f2} = 4.18D_S^{-1.17}, \tag{4.12}$$

while

$$\sigma_{f2} = (\sqrt{2\pi}H_{f2})^{-1}. \tag{4.13}$$

The third part of the total filament number density function, $P_{f3}(D_i)$, comes from the disintegration of the connecting bridge of water formed as the two main fragments separate. The best fit for the fragment size distributions of all 10 collision pairs for this fragment type was by a log-normal curve with the parameters calculated in much the same fashion as those for the Gaussian portions of the distribution. The mode D_{ff3} was a linear function of the small drop size only, i.e.,

$$D_{ff3} = 0.241D_S + 0.0129. \tag{4.14}$$

Since one drop fragment is removed each for large drop and small drop as remnants of the original pair, the average fragment number is $\bar{F}_f - 2$, as represented by the area under P_{f3}. For a log-normal distribution, the density function is

$$P_{f3}(D_i) = \frac{H_{f3}}{D_i}\exp\left[-\frac{1}{2}\left(\frac{\ln D_i - \mu_{f3}}{\sigma_{f3}}\right)^2\right], \tag{4.15}$$

where H_{f3} is a constant indicative of height, σ_{f3} is a measure of the spread, and μ_{f3} is the natural logarithm of the median value. σ_{f3} is related to the mode by

$$\mu_{f3} = \ln D_{ff3} + \sigma_{f3}^2. \tag{4.16}$$

At the modal value $D_i = D_{ff3}$. Thus

$$P_{f3}(D_{ff3}) = \frac{H_{f3}}{D_{ff3}}\exp(-0.5\sigma_{f3}^2). \tag{4.17}$$

This represents the maximum value $P_{f3,0}$ of the density curve which was found to be dependent on both D_L and D_S. $P_{f3,0}$ is decomposed into three parts:

$$P_{f3,01} = 1.68 \times 10^5 D_S^{2.33}, \tag{4.18}$$

for $D_S \leq D_{S0}$;

$$P_{f3,02} = [43.4(D_L + 1.81)^2 - 159.0]D_S^{-1} - 3870(D_L - 0.285)^2 - 58.1, \tag{4.19}$$

for $D_S \geq 1.2D_{S0}$; and

$$P_{f3,03} = \alpha P_{f3,01} + (1 - \alpha)P_{f3,02}, \tag{4.20}$$

for $D_{S0} < D_S < 1.2D_{S0}$. D_{S0} is obtained from Eq. (3.5) and

$$\alpha = (D_S - D_{S0}) \times (0.2D_{S0})^{-1}. \tag{4.21}$$

The values of σ_{f3} are obtainable in a manner similar to that for σ_{f1}. As the fragment measurements had a lower cutoff in resolution at $D_0 = 0.01$ cm (0.05 cm for the data of M-L), the integration of Eq. (4.15) from D_0 to infinity is equal to $\bar{F}_f - 2$. With an initial guess of

$$\sigma_{f3,1} = 10D_{ff3} \tag{4.22}$$

and

$$\sigma_{f3,i+1} = \sqrt{\frac{2}{\pi}}\left(\frac{\bar{F}_f - 2}{H_{f3}}\right) \times \left[1 - \text{erf}\left(\frac{\ln D_0 - \mu_{f3}}{\sqrt{2}\sigma_{f3,i}}\right)\right]^{-1}, \tag{4.23}$$

σ_{f3} can be iteratively solved and used to find H_{f3} and μ_{f3}. The total filament density function can then be expressed as

$$P_{fi}(D_i) = P_{f1}(D_i) + P_{f2}(D_i) + P_{f3}(D_i). \tag{4.24}$$

The results of these calculations are superimposed onto graphs of the experimental results in Figs. 11–13 of LL for all the drop pairs studied. Thereby, $P_{fi}(D_i)$ is expressed as an average number of fragments of diameter D_i per 0.01 cm size interval. The total area under each curve is $\bar{F}_f$. The experimental values are plotted as histograms. Each bar of the histogram is centered at the drop size measured and the width is indicative of the size interval resolved. Vertical bars indicating the standard deviation of each measurement are given only for the 0.18 and 0.0395 cm pair but are representative of the deviations found for the others. The comparison shows agreement between the data and the parameterized values within the bounds of experimental fluctuation for the collision values over the whole range of fragments sizes measured. For collisions where $D_S = 0.0395$ cm, the numbers of filament breakup per size interval also represents the overall breakup as breakup occurred only via the filament configuration.

b. Sheet breakup

The sheet type of breakup is easier to represent than the filament type because it is composed of only two parts. The density function $P_{s1}(D_i)$ gives the distribution of the large drop fragment around D_L, and a single function $P_{s2}(D_i)$ can describe the rest of the fragments. In a sheet collision, the small drop is no longer recognizable among the fragments. $P_{s1}(D_i)$ can again be represented by a Gaussian as for the filaments, so that

$$P_{s1}(D_i) = H_{s1} \exp\left[-0.5\left(\frac{D_i - D_L}{\sigma_{s1}}\right)^2\right] \tag{4.25}$$

is centered at D_L with heights of H_{s1} and a spread of σ_{s1}. The upper cutoff of D_{coal} and an integral of 1 allows Eq. (4.10) to be used as solutions for σ_{s1} with a substitution of H_{s1} for H_{f1}. H_{s1} was found to be a simple exponential function of the small drop size, i.e.,

$$H_{s1} = 100 \exp(-3.25D_S). \tag{4.26}$$

This implies that the removal of mass from D_L in a sheet depends only on the energy or momentum per unit diameter of D_S that is applied to the large drop in the shearing action of the collision.

The cloud droplet part of the fragment number distribution is represented by another log-normal relation peaking at a modal value of

$$D_{ss2} = 0.254D_S^{0.413} \exp[3.53D_S^{-2.51}(D_L - D_S)]. \tag{4.27}$$

This peak is generally at values less than D_S and approaches the small drop size as the difference between the colliding drops decreases. The height of this peak, H_{s2}, is obtained from

$$P_{s2}(D_{ss2}) = \frac{H_{s2}}{D_{ss2}} \exp(-0.5\sigma_{s2}^2). \tag{4.28}$$

The data showed

$$P_{s2}(D_{ss2}) = 0.23D_S^{-3.93}D_L^{b^*}, \tag{4.29}$$

where

$$b^* = 14.2 \exp(-17.2D_S). \tag{4.30}$$

With Eqs. (4.27)–(4.30) the parameters of the log-normal curve are given by the integral expression

$$\int_{D_0}^{\infty} \frac{H_{s2}}{D_i} \exp\left[-0.5\left(\frac{\ln D_i - \mu_{s2}}{\sigma_{s2}}\right)^2\right] dD_i = \bar{F}_s - 1, \tag{4.31}$$

where

$$\mu_{s2} = \ln D_{ss2} + \sigma_{s2}^2 \tag{4.32}$$

and $\bar{F}_s$ is from Eq. (3.7). σ_{s2} is found as σ_{f3} was from Eqs. (4.22) and (4.23).

The results of $P_{s1}(D_i)$ and $P_{s2}(D_i)$ are given in full in Fig. 12 of LL and in comparison with the experimental data. The overall agreement is satisfactory. The experimental values using $D_L = 0.18$ cm are not as reliable as the other sheet results because of the small number of collisions (C_s) observed in these two series. The total number of fragments analyzed was <30 in both cases.

c. Disk breakup

The disk type of drop breakup is limited to collisions involving higher values of CKE and is the most violent form of collision. It generally occurs in an attempt at dissipating the high kinetic energy by conversion into surface energy. The approximation to a disk-like plate also ensures a high drag coefficient. The transfer of energy and momentum into the

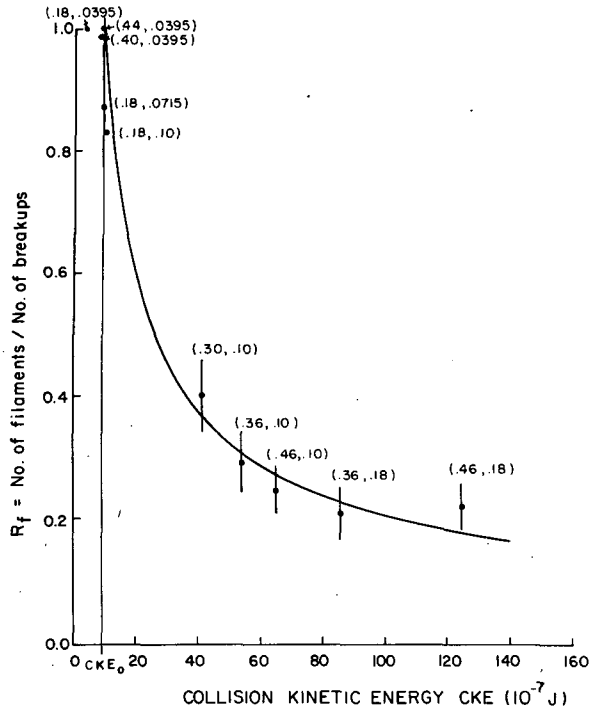

FIG. 1. Contribution to overall breakup by each filament collision as a function of the collision kinetic energy CKE; vertical bars indicate errors. All breakup at CKE < CKE$_0$ = 0.893 μJ occurs as filaments.

surrounding air through friction is greater for disks than for sheets or filaments. Disks exhibit the most severe oscillations of the drop mass after initial contact, hence it also has the highest loss of energy through internal viscosity.

The fragments produced through disks can be described in a manner similar to the results for sheets: the outcome of each collision is usually composed of one main large fragment and many small ones. With the severity of this collision type, even the largest fragment produced is sometimes not distinctly recognizable as the remainder of the large colliding drop. As a result, the fragment density around D_L can be represented as a Gaussian function $P_{d1}(D_i)$ but the mode is now shifted below the value of D_L. The large drop is broken into more fragments if the energies of the collision are greater.

To locate this peak, the disks were analyzed in terms of their kinetic and surface energies. If a Weber number of the energies [J] is defined as

$$W_1 = \text{CKE} \times S_C^{-1}, \tag{4.33}$$

where S_C is the surface energy of the coalesced drop $[=\pi\sigma(D_L^3 + D_S^3)^{2/3}]$. Then the value of the mode for the Gaussian function can be described by

$$D_{dd1} = D_L\{1 - \exp[-3.70(3.10 - W_1)]\}. \tag{4.34}$$

The number density function becomes

$$P_{d1}(D_i) = H_{d1} \exp\left[-0.5\left(\frac{D_i - D_{dd1}}{\sigma_{d1}}\right)^2\right], \tag{4.35}$$

with the area under $P_{d1}(D_i)$, integrated along D_i from 0 to D_{coal}, equal to 1. The height of this distribution is directly related to CKE by

$$H_{d1} = 1.58 \times 10^{-5}\ \text{CKE}^{-1.22}. \tag{4.36}$$

σ_{d1} is found through iteration again.

The remainder of the fragments can be described by a log-normal approximation, just as in the sheet breakup, but with different values for the distribution parameters. The mode D_{dd2} of $P_{d2}(D_i)$ is dependent on the sizes of the colliding drops and is located to the left of D_S with

$$D_{dd2} = \exp[-17.4D_S - 0.671(D_L - D_S)]D_S\,. \tag{4.37}$$

The height is found from

$$P_{d2}(D_{dd2}) = \frac{H_{d2}}{D_{dd2}} \exp(-0.5\sigma_{d2}{}^2)$$

$$= 0.0884D_S^{-2.52}(D_L - D_S)^{b^*}, \tag{4.38}$$

where

$$b^* = 0.007D_S^{-2.54}\,. \tag{4.39}$$

Integration of the log-normal function $P_{d2}(D_i)$ is equal to $\bar{F}_d - 1$. σ_{d2} can be found as in the log-normal functions for the filaments and sheets. The results for the parameterized disk distributions can be found in Fig. 13 of LL.

d. Overall breakup

The sum of the expressions of Sections 4a–4c, describing the individual breakup types, gives the overall fragment number densities for breakup according to Eq. (2.6), once the contribution of each breakup type is known. The fraction of all breakups that occurred as filaments was found to be

$$R_f = \begin{cases} 1.11 \times 10^{-4}\ \text{CKE}^{-0.654}, & \\ \qquad\qquad \text{for} \quad \text{CKE} \geqslant \text{CKE}_0\,, & (4.40) \\ 1.0, \qquad \text{for} \quad \text{CKE} < \text{CKE}_0\,. & (4.41) \end{cases}$$

For CKE greater than a lower limit of CKE$_0$ = 89.3 μJ, R_f obeys the power law of Eq. (4.40), but when the collision energy decreases below this value all breakup is postulated to occur by way of filament formation. The above expression compares with the measurements according to Fig. 1.

Similarly, there is a specific contribution to the overall breakup by sheets. This fraction is approximately a function of the ratio W_2 of the CKE to the sum of the surface energies of the two original drops

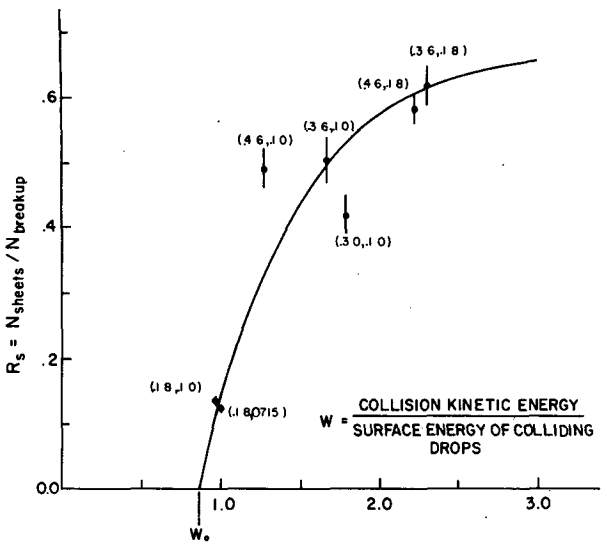

FIG. 2. Contribution to overall breakup by each sheet collision, as function of a Weber number W (ratio between collision kinetic energy and surface tension energy). No sheet breakup occurs for $W < W_0 = 0.86$.

or

$$W = \mathrm{CKE}\, S_T^{-1}. \tag{4.42}$$

Thus the fraction of the sheets formed in all the breakups is given by

$$R_s = \begin{cases} 0.685\{1 - \exp[-1.63(W_2 - W_0)]\}, & \\ \qquad\qquad \text{for} \quad W \geq W_0 = 0.86, & (4.43) \\ 0, \qquad\qquad \text{for} \quad W < W_0\,. & (4.44) \end{cases}$$

W_0 is the lower limit below which no sheet collisions occurred. R_s is depicted in Fig. 2 together with the experimental values.

With Eqs. (4.40), (4.41), (4.43) and (4.44) giving values for R_f and R_s, the fractional contribution of the disk to overall breakup is given by

$$R_d = \begin{cases} 1 - (R_f + R_s), & \text{for} \quad R_f + R_s \leq 1.0, \quad (4.45) \\ 0, & \text{for} \quad R_f + R_s > 1.0. \quad (4.46) \end{cases}$$

There is a need for the latter condition to preserve physical reality in extreme situations. A summary of each breakup fraction is given in Table 2.

e. *Overall breakup in all collisions*

To arrive at the overall fragment number distributions for an average collision the values of $P_b(D_i)$ must be modified by the fraction of total collisions which produce two or more fragments. This breakup efficiency is given by $(1 - E_{\mathrm{coal}})$, so that overall equation is

$$P_i(D_i) = [R_f P_f(D_i) + R_s P_s(D_i) + R_d P_d(D_i)] \times [1 - E_{\mathrm{coal}}] + \delta(D_{\mathrm{coal}}) E_{\mathrm{coal}}\,. \tag{4.47}$$

The first part of Eq. (4.47) is the breakup portion while the second part is from coalescence. [E_{coal} was parameterized by LL in their Eq. (4.5)]. The coalescence portion is evaluated as a Dirac delta function expressed by

$$\delta(D_{\mathrm{coal}}) = 1, \quad \text{for} \quad D_i = D_{\mathrm{coal}}\,, \qquad = 0 \quad \text{otherwise.} \tag{4.48}$$

In a discrete representation, the coalescence contribution can be shown by a bar on a histogram of arbitrary height or width, centered on D_{coal} with the area of the bar equal to E_{coal}.

Eq. (4.47) is plotted in Fig. 3. The smooth curves give the breakup with the bar centered at the upper cutoff point of the fragment sizes indicating the coalescence contribution. The widths of the coalescence bar were chosen to represent the experimental error in the D_{coal}. The dashed lines give the measured frag-

TABLE 2. Comparison of experimentally measured and calculated (by parameterization) fractions R_j of all collisions (including the ones leading to coalescence) resulting in breakup; drop pairs are listed in increasing magnitude of the collision kinetic energy. R_f stands for filament, R_s for sheet and R_d for disk configurations in breakup.

No.	Drop pair diameters (cm)	R_f		R_s		R_d	
		Calculated	Experimental	Calculated	Experimental	Calculated	Experimental
1	0.18 & 0.0395	1.0	1.0	0.0	0.0	0.0	0.0
2	0.40 & 0.0395	1.0	0.99	0.0	0.013	0.0	0.0
3	0.44 & 0.0395	1.0	1.0	0.0	0.0	0.0	0.0
4	0.18 & 0.0715	1.0	0.87	0.18	0.13	0.0	0.0
5	0.18 & 0.10	0.96	0.83	0.12	0.14	0.0	0.031
6	0.30 & 0.10	0.37	0.41	0.53	0.42	0.096	0.14
7	0.36 & 0.10	0.31	0.29	0.50	0.51	0.19	0.19
8	0.46 & 0.10	0.27	0.25	0.34	0.49	0.39	0.20
9	0.36 & 0.18	0.23	0.21	0.62	0.62	0.15	0.14
10	0.46 & 0.18	0.18	0.22	0.61	0.59	0.21	0.17

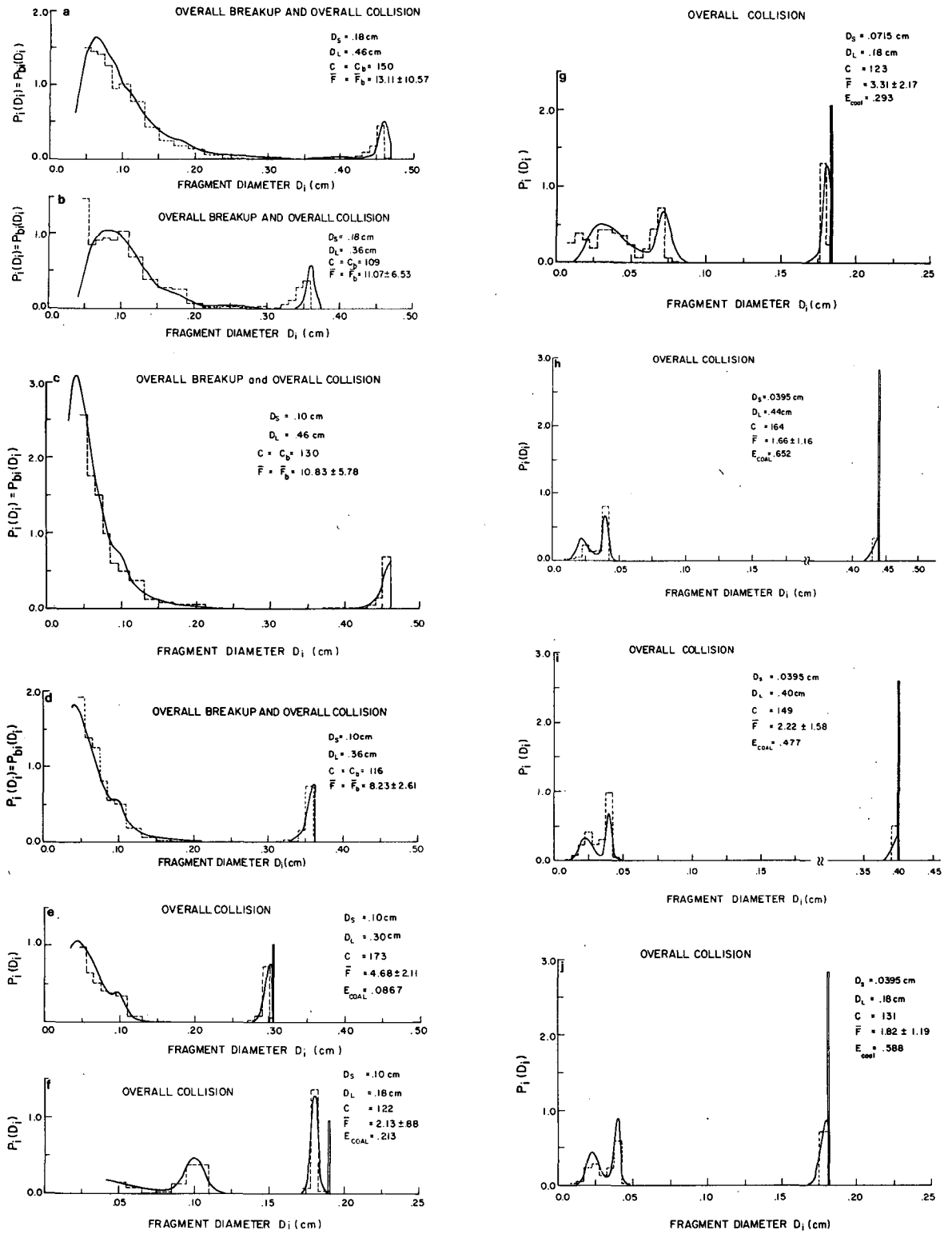

FIG. 3. Histograms of measured and line diagrams of calculated (through parameterization) fragment numbers $P_i(D_i)$ for overall collisions, as a function of the fragment diameter D_i, for 10 different drop pairs. $P_i(D_i)$ represents the average outcome of one collision and is obtained by scaling the overall (average) breakup by the coalescence efficiency E_{coal} through the factor $(1 - E_{coal})$. The bar at the cutoff is the contribution from coalesced drops, its area is equal to E_{coal}. C is the number of drop pairs in any given series. Diagrams without the "coalescence bar" indicate zero coalescence efficiency, i.e., in these cases the overall collision outcome is the same as the overall breakup. Diagrams are arranged in descending order of collision kinetic energy CKE.

ment number distributions as histograms. For the cases where there was no coalescence, the overall fragment size distributions for collisions are equal to the distributions for overall breakup, i.e., the cases for $E_{coal} = 0$ [see Eq. (4.47)].

5. Discussion of results

A test of the calculations for the individual fragment number distributions and for the coalescence efficiencies is the comparison of the overall fragment numbers calculated for an average collision to the experimental measurements. The collisions were analyzed by partitioning them into breakup types and summing up of the fragment numbers. From all collisions, this average number is given by

$$\bar{F} = (R_f\bar{F}_f + R_s\bar{F}_s + R_d\bar{F}_d)(1 - E_{coal}) + E_{coal}\,. \quad (5.1)$$

The calculated and measured values of $\bar{F}$ for all 10 pairs are given in Table 3. The agreement between the two sets of numbers is good, i.e., even better than the error bars would indicate. Instead of adding the standard deviations, taking root mean squares may have indicated a much more realistic accuracy.

The parameterized curves also allow extrapolation to other sizes. The application of Eq. (5.1) is shown in Fig. 4 for two large drop diameters. Although the experiments of LL did not utilize small drops > 0.18 cm in diameter, the results of the extrapolation seem justified also in this region. As D_S approaches D_L it is expected that breakup decreases. As CKE lessens due to the low impact velocity, the drops would tend to merge or just form two drops as fragments if breakup occurs. The value for $\bar{F}$ in such cases would be $2 - E_{coal}$. Studies by Vaughan and Hill (1974) and Vaughan *et al.* (1974) of very large drop collisions at zero *g* aboard Skylab 4 tend to support this argument, even though the conditions were far from atmospheric. Likewise, at small D_S where D_L becomes much greater than D_S, a similar situation occurs, as shown by Whelpdale and List (1971) and Levin and Machness (1977). At both extremes, the value for $\bar{F}$ must reach a value lying between 1 and 2, as shown by Fig. 4. The trends indicate that the extrapolations follow some physical expectations. Notice that these curves form a three-dimensional surface if plotted for all D_L. They are not based only on the five points shown but on other five points with different D_L.

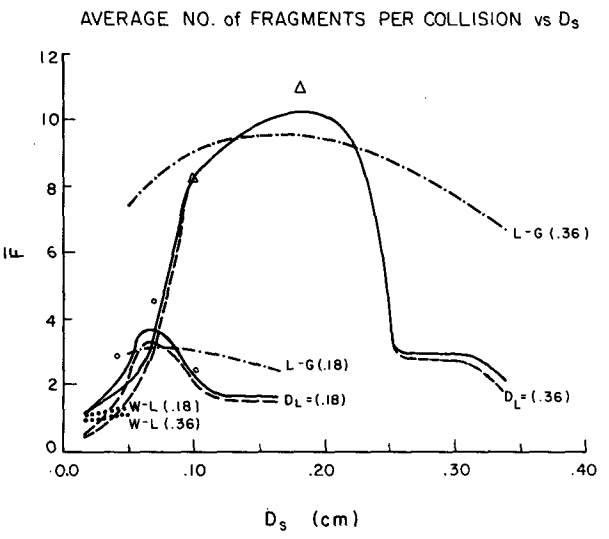

FIG. 4. Average number of fragments per collision as calculated through parameterization as a function of the small drop diameter D_S, for two values of D_L (0.36 and 0.18 cm diameter); solid curve is for overall $\bar{F}$, dashed line for breakup ($\bar{F}_b$) only. Measured data points are triangles for D_L = 0.36 cm, circles for D_L = 0.18 cm. Earlier parameterization by List and Gillespie (1976) are given by curves designated L-G, those by Whelpdale and List (1971) W-L.

In between the limits of large D_L/D_S and $D_L/D_S \approx 1$, the curves rise according to the contributions to the overall fragment number by each of the modes of breakup. For example, in examining the $\bar{F}$ curve for D_L = 0.36 cm, the slow increase as D_S decreases to 0.25 cm from D_L is attributable to fragmentation from filament breakup. As CKE increases further, the disk and sheet shapes begin to appear, which is reflected in the rapid rise at 0.25 cm. As D_S decreases below 0.10 cm, the fragment numbers are again primarily the result of filament breakup and coalescence and $\bar{F}$ again decreases to values between 1 and 2. The same is true with the D_L = 0.18 cm curve. Both the overall fragment numbers (based on all collisions) and the fragments due to breakup alone are given in Fig. 4 to show the effects of coalescence. Notice that according to Eq. (5.1) the breakup and coalescence number can be >2 because it is weighted by $(1 - E_{coal})$.

$\bar{F}$ also provides a good means of comparison between these results and those of other parameteri-

TABLE 3. Comparison of experimentally measured and calculated (by parameterization) average fragment numbers $\bar{F}$ per collision, as averaged over all collisions of each drop pair; $\bar{F}$ is based on all breakups and coalescences.

No.	Drop pair diameters (cm)	$\bar{F}$ Calculated*	$\bar{F}$ Experimental
1	0.18 & 0.0395	2.02	1.82 ± 1.19
2	0.40 & 0.0395	1.79	2.22 ± 1.58
3	0.44 & 0.0395	1.76	1.66 ± 1.16
4	0.18 & 0.0715	3.67	3.31 ± 2.17
5	0.18 & 0.10	2.24	2.13 ± 0.88
6	0.30 & 0.10	5.06	4.68 ± 2.11
7	0.36 & 0.10	8.11	8.23 ± 2.61
8	0.46 & 0.10	11.47	10.83 ± 5.78
9	0.36 & 0.18	10.33	11.07 ± 6.53
10	0.46 & 0.18	14.20	13.11 ± 10.57

* Including coalescence; if any.

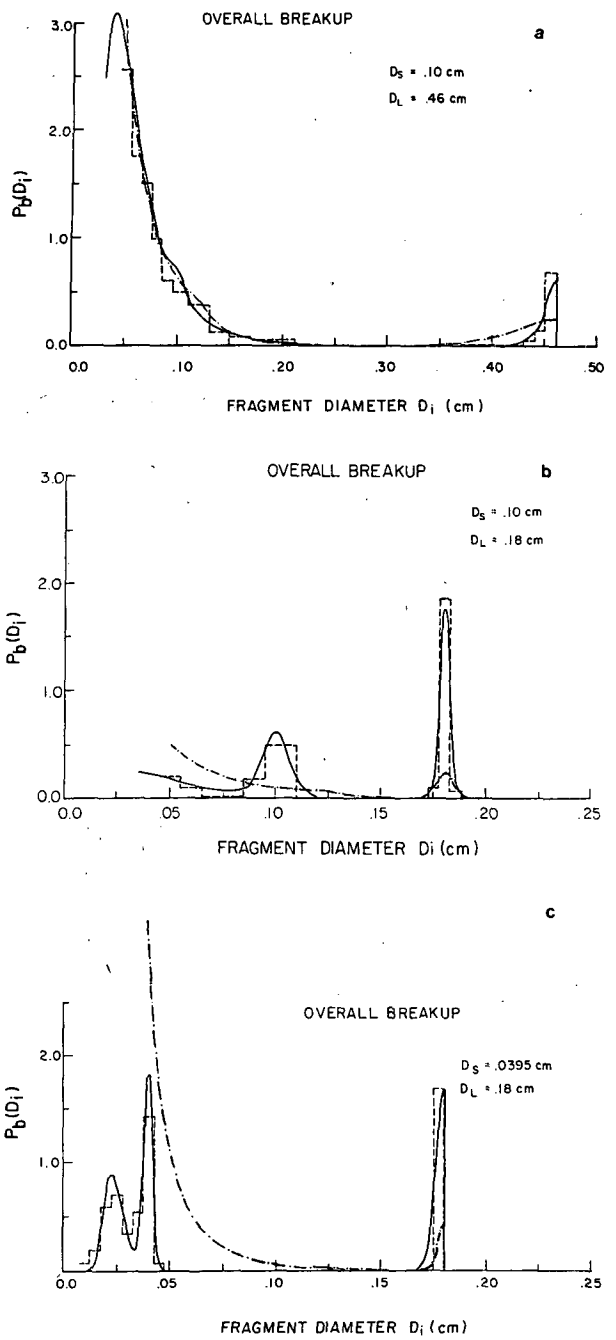

FIG. 5. Three comparisons of overall breakup parameterization by List and Gillespie (1976) (dash-dotted line) with present work (solid line) and histograms of experimentally determined values (dashed line). Note inability of the List-Gillespie scheme to properly describe distributions of small fragments due to insufficient resolution of small fragments in earlier experiments by M-L (dash-dotted).

zation schemes for drop collisions. Hence, the fragment number distributions for overall breakup, as calculated in this study for three of the experimental drop pairs, are shown in Figs. 5a–5c, and are compared to the hitherto most elaborately parameterized values of List and Gillespie (1976), as transformed into diameter coordinates. Fig. 5a for the [0.46; 0.10 cm] drop pair shows good agreement for the small fragments measured, but the distribution for the large fragment diameters was too broad and too low. One reason for this discrepancy was a deficiency in resolving this fragment size in the earlier measurements. The earlier results had a discontinuity at 0.05 cm due to the limited resolution of the data. Consequently, these values are only representative, in the average, of the middle range of drop sizes. Both sets of results, however, are compatible and the agreement obtained after totally independent derivations increases confidence in both sets of results.

Fig. 5b shows the same calculations for the [0.18; 0.10 cm] pair which was still within the bounds of the calculations by List and Gillespie (1976) and Gillespie and List (1978/79), but shows the beginning of significant inaccuracies in their parameterization scheme. The peak of D_S was not perceived and the existence of the large fragment peaked at D_L was much stronger than anticipated.

Fig. 5c for the [0.18; 0.0395 cm] pair shows total breakdown as the calculations based on the early data set are too high by four orders of magnitude for the 0.10 cm diameter fragment, if extrapolated to that size. Discrepancies are also present, although to a lesser degree, for the rest of the spectrum. This comparison shows the importance of the experimentally caused cutoff at 0.05 cm which affected List and Gillespie (1976) and Gillespie and List (1978/79) in their modeling.

The problem in the fitting of the number distribution curves to breakup data is that the distribution functions need to be general and apply to all pairs measured in order to give confidence to interpolations as well as extrapolations. For this purpose, the calculated fragment probabilities were shown in comparison to the measured values. Other tests of statistical significance—such as the χ^2 test—are based on a normal distribution of errors and are not applicable. The errors and the numbers of fragments produced in each collision are not normally distributed, but rather tend to be either positively or negatively skewed toward the larger drop sizes and are interdependent through nonlinear relationships.

Each fragment number distribution represents a two-dimensional relationship resulting from a collision between a particular drop pair. Each drop pair in turn is a single point extracted from a plane of infinite combinations of drop sizes with axes D_L and D_S. Thus the fragment numbers per size interval are represented by a four-dimensional surface. No topological and/or statistical techniques are available at present to solve the problem of statistical testing. However, comparisons showed that the applied subjective superpositioning of the parameterized distributions onto the experimental data is quite adequate.

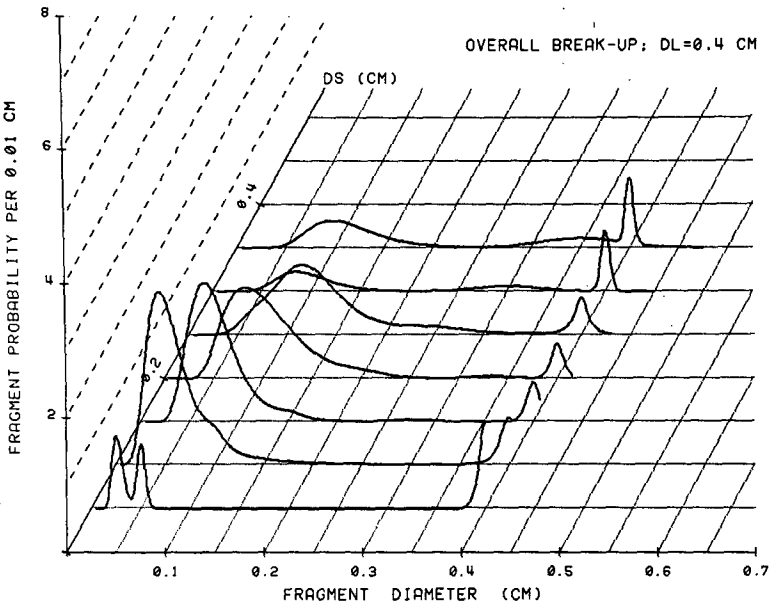

FIG. 6. Average fragment number distributions for overall breakup, for different small drop diameters D_S, for a large drop diameter D_L = 0.40 cm. Note the small ridge of fragments echoing the original small drop approaching the large fragments (remnants of the large drops D_L) for $D_S \rightarrow D_L$, and the independent ridge of the smaller fragments.

The reduction of the four-dimensional relations to three dimensions by the selection of a single large drop size allows the visualization of effects of collisions between the single large drop with all other small ones. This three-dimensional representation of the fragment number density for filament breakup is given in Fig. 6 for D_L = 0.4 cm. It shows the effect of varying the size of the small drop on the fragment number distribution. For an infinite number of smaller drops rather than the incremental ones shown, the number distribution would be represented by a contoured surface. Such three-dimensional surfaces will be explored in Part III of this series of papers (List *et al.*, 1982).

The usage of the breakup fragment size distributions in the modeling of rain formation should provide a better insight into the evolution of precipitation and throw some light on the limitations of drop sizes. It is thereby necessary to realize some of the limitations of the experiments of LL and the parameterization applied in the present paper. First, the resolution into fragment bins is related to the number of experiments carried out. There is no point in having categories which are too fine if there are not enough fragments belonging to them. One hundred breakups were set as a minimum and seem adequate for the fragment numbers observed and bin variations considered. It is also clear that it would not make sense to overdo this breakdown because any numerical simulation would not use any finer mesh because of the limitations to computing power.

The breakup situation seems somewhat crucial for the large fragments where an indication about their exact sizes relative to the original large drop diameter is needed in order to indicate if there is a growth in the average or not. One of the weaknesses of the parameterization is that it was applied to diameter (which was measured) and not to mass. Hence the centering of the Gaussians for the large fragments at D_L (for filaments and sheets) implies that the mass of the average large fragment is larger than that of the original large drop because of the skewness introduced by the diameter representation. When it comes to numerical modeling this skewness increases because the mass scale is even more distorted by the bin size increase normally chosen with increasing particle size. All these aspects play a role in the recognition of raindrop spectra evolving to equilibrium distributions as proposed by Gillespie and List (1978/79). However, they do not entirely control the outcome because in some breakups no large fragments echo the original large drop. Further, the growth by collection of small cloud droplets between breakup needs to be considered too because it compensates for some of the large drop losses in breakup (for disks).

The experiments underlying the parameterization obviously conserved mass. The parameterization however, was not forced to conserve mass. But it was fine-tuned to do it with good accuracy [one numerical model test run regarding the evolution of a Marshall-Palmer size distribution in a one-dimensional shaft

model of the type Gillespie and List (1978/79) used conserved mass flux within 0.07% during a fall over 2 km]. The possibility of using different bin sizes from the ones chosen in this paper would certainly affect mathematically forced mass conservation. It is therefore suggested that such mass conservation schemes be applied in numerical models once the bin size sequence has been set.

6. Summary and comments

The collision results of Low and List (1982) utilizing 10 combinations of representative raindrop sizes were parameterized for use in cloud modeling. The curves fitted to describe average events were arrived at in the following manner: The collisions were subdivided into three different categories according to the geometric shape assumed by the drops after contact. These were defined as filaments, sheets and disks. The average numbers of a particular fragment size occurring in an experiment were plotted as histograms and fitted by a sum of normal and lognormal distributions. The parameters of each distribution were related to basic variables of the experiments, i.e., large and small drop diameters through diameter combinations as expressed in the collision kinetic energy of impact in the center of mass frame and the surface energies of the individual and combined drops.

The frequency of occurrence of each breakup type was used as a weighting function to determine the contribution of each mode of breakup to the net fragmentation rate. By combining breakup with coalescence efficiency as determined by Low and List (1982), the overall effect of any two raindrops colliding in free fall was found. This parameterization of the collision, coalescence and breakup data should become very valuable in the numerical modeling of precipitation processes. Such modeling efforts are presently under way and will be reported later, beginning in Part III of this paper (List *et al.* 1982).

Previous studies by other authors into raindrop collisions were not carried out under conditions with parallel vectors for velocity, total drag and gravity. Thus, it is of no surprise that the developed criteria for breakup and the fragment numbers produced based on angular momentum (Brazier-Smith *et al.* (1972), collision energetics (Lee and Dingle, 1978), and relative impact velocities (Bradley and Stow, 1979) are inadequate and showed no consistent pattern when applied to the new data set taken under free fall conditions.

Acknowledgment. The authors are grateful for the sponsoring of this research by the Atmospheric Environment Service of Canada.

REFERENCES

Bradley, S. G., and C. D. Stow, 1979: On the production of satellite droplets during collisions between water drops falling in still air. *J. Atmos. Sci.*, **36,** 494–500.

Brazier-Smith, P. R., S. G. Jennings and J. Latham, 1972: The interaction of falling water drops: coalescence. *Proc. Roy. Soc. London*, **A326,** 393–408.

Gillespie, J. R., and R. List, 1978/79: Effects of collision-induced breakup on drop size distributions in steady rainshafts. *Pure Appl. Geophys.*, **117,** 599–626.

Lee, Y., and A. N. Dingle, 1978: Raindrop breakup: The energy of disruption. *Preprints Cloud Physics Conf.*, Issaquah, Amer. Meteor. Soc., 129–132.

Levin, Z., and B. Machnes, 1977: Experimental evaluation of the coalescence efficiencies of colliding water drops. *Pure Appl. Geophys.*, **115,** 845–867.

List, R., and J. R. Gillespie, 1976: Evolution of raindrop spectra with collision-induced breakup. *J. Atmos. Sci.*, **33,** 2007–2013.

——, and C. Fung, 1982: The effect of pressure on the breakup of one pair of raindrops. *Atmos.–Oceans,* **20,** 17–27.

——, E. Freire, A. Ashton, N. Donaldson, T. B. Low and J. R. Gillespie, 1982: Collision, coalescence and breakup of raindrops. Part III: Generalization of parameterization and application to a rainshaft (in preparation).

Low, T. B., 1977: Products of interacting raindrops, experiments and parameterization. Ph.D. thesis, University of Toronto, 230 pp.

——, and R. List, 1982: Collision, coalescence and breakup of raindrops, Part I: Experimentally established coalescence efficiencies and fragment size distributions in breakup. *J. Atmos. Sci.*, **39,** 1591–1606.

McTaggart-Cowan, J. D., and R. List, 1975: Collision and breakup of water drops at terminal velocity. *J. Atmos. Sci.*, **32,** 1401–1411.

Vaughan, O. H., and C. K. Hill, 1974: Drop coalescence in zero-gravity environment of Skylab IV. *Bull. Amer. Meteor. Soc.*, **55,** 1127–1130.

——, R. E. Smith and R. J. Hung, 1974: Skylab fluid mechanics demonstration: a study of water droplet oscillations in space. *Preprints Cloud Physics Conf.*, Tucson, Amer. Meteor. Soc., 408–411.

Whelpdale, D. M., and R. List, 1971: The coalescence process of raindrop growth. *J. Geophys. Res.*, **76,** 2836–2856.